

End-to-end Autoencoder for Superchannel Transceivers with Hardware Impairment

Jinxiang Song⁽¹⁾, Christian Häger⁽¹⁾, Jochen Schröder⁽²⁾,
Alexandre Graell i Amat⁽¹⁾, and Henk Wymeersch⁽¹⁾

⁽¹⁾ Department of Electrical Engineering, Chalmers University of Technology, Gothenburg, Sweden

⁽²⁾ Department of Microtechnology and Nanoscience, Chalmers University of Technology, Gothenburg, Sweden

jinxiang@chalmers.se

Abstract: We propose an end-to-end learning-based approach for superchannel systems impaired by non-ideal hardware component. Our system achieves up to 60% SER reduction and up to 50% guard band reduction compared with the considered baseline scheme.

© 2021 The Author(s)

1. Introduction

Modern high spectral efficiency (SE) superchannel systems require dense channel spacing (close to the symbol rate) coupled with high-order modulation formats. The narrow channel spacing and high-order modulation formats, however, exacerbate performance degradation due to non-ideal hardware components [1, 2]. To compensate for the hardware impairments, various digital pre-distortion (DPD) algorithms including arcsin [3, 4] and Volterra series-based pre-compensation [5–8] have been proposed.

As an alternative to these conventional approaches, deep learning (DL) techniques using neural networks (NNs) have recently been proposed for hardware impairment compensation in both wireless [9–12] and optical communications [13–17], where the main idea is to replace the DPD block with an NN that can be optimized from data. In contrast to focusing on a specific functional block (e.g., DPD), end-to-end learning using an autoencoder (AE) optimizes the transmitter and receiver jointly [18]. However, the methods in [9–17] are derived considering a single-channel setup, thus ignoring inter-channel interference (ICI) with neighboring channels, which can yield significant performance degradation in densely-spaced superchannel systems.

In this paper, we propose a novel end-to-end AE for superchannel systems impaired by non-ideal hardware component, the nonlinear IQ-Modulator (IQM) in particular, that limits ICI. Simulation results show that our method achieves significantly better symbol error rate (SER) performance than a conventional baseline scheme. Moreover, the proposed approach shows great potential to increase the SE of superchannel systems by reducing the guard band with limited impact on the SER.

2. System model

Fig. 1 depicts the considered superchannel system. For each channel, messages belonging to the set $\mathcal{M} = \{1, \dots, M\}$ are mapped to constellation points belonging to the set $\mathcal{X} = \{x_1, \dots, x_M\}$. The upsampled signals are convolved with a pulse-shaping (PS) filter, after which a DPD algorithm is applied to pre-compensate for the IQM nonlinearity. The pre-compensated signal is then fed to the digital-to-analog converter (DAC) and amplified by a linear electrical power amplifier (PA) to drive the IQM. Similar to [3, 5, 6], we consider a back-to-back setup, where additive white Gaussian noise (AWGN) with constant power is added to simulate the noise introduced by the booster amplifier. At the receiver, the received signals are passed through an analog-to-digital converter (ADC) and then convolved with a matched filter (MF). Finally, the downsampled signals are mapped to estimates of the transmitted messages.

3. AE-based superchannel system

In principle, the entire transmitter and receiver can be implemented as an AE and optimized by end-to-end learning as proposed in [18]. However, this will lead to i) a black-box solution that can be difficult to interpret and ii) potentially high training complexity (a very complex transmitter NN with large memory may be required). To address both issues, we follow a different approach where the transmitter NN is decomposed into a concatenation of simpler NNs, each corresponding to one functional block of a conventional communication system. By doing this, an additional advantage is that the parameters of these NNs can be initialized such that they initially perform

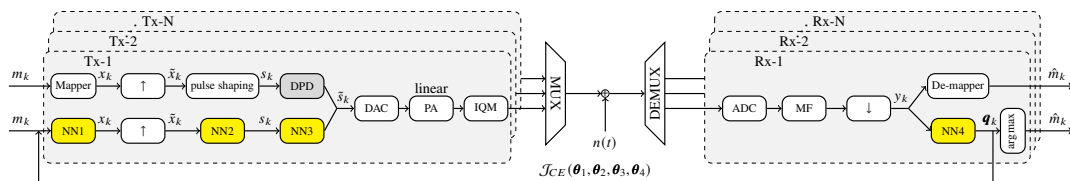


Fig. 1. Block diagram showing the end-to-end system model (\uparrow : upsampling, \downarrow : downsampling). The top branch corresponds to the conventional baseline scheme and the bottom branch to the proposed AE learning-based scheme.

close to their conventional counterparts. As a result, the proposed scheme has *increased interpretability* and *decreased training complexity* as compared to a conventional AE. We note that a similar approach has recently been applied for nonlinear optical channels in [19], where the transmitter implementation includes a trainable symbol mapper and a trainable PS filter, and it has been show that a PS filter can be trained to compensate the chromatic dispersion and Kerr nonlinearity.

3.1. Proposed trainable AE

As shown in the bottom branch of Fig. 1, the AE transmitter is implemented as a concatenation of three NNs. These NNs are denoted by $f_{\theta_1}(\cdot)$, $f_{\theta_2}(\cdot)$, $f_{\theta_3}(\cdot)$, where θ_1, θ_2 , and θ_3 are the sets of trainable parameters, and are defined as follows:

- NN1 $f_{\theta_1}: \mathcal{M} \rightarrow \mathbb{C}$ maps a given message $m_k \in \mathcal{M}$ to a constellation point according to $x_k = f_{\theta_1}(m_k)$, where an average power constraint $\mathbb{E}\{|x_k|^2\} = 1$ is enforced by a normalization layer [18].
- NN2 $f_{\theta_2}: \mathbb{C}^N \rightarrow \mathbb{C}$ generates the pulse-shaped signal according to $s_k = \theta_2^\top \tilde{\mathbf{x}}_k$, where $\tilde{\mathbf{x}}_k = [\tilde{x}_{k-N}, \dots, \tilde{x}_k]^\top$ is a sequence of N complex-valued input signals. Note that NN2 only has a single layer applying a linear activation function, and can be interpreted as a standard finite impulse response filter.
- NN3 $f_{\theta_3}: \mathbb{C} \rightarrow \mathbb{C}$ generates the pre-distorted signal according to $\tilde{s}_k = f_{\theta_3}(s'_k)$, where $f_{\theta_3}(\cdot)$ operates separately on the in-phase and quadrature branches, and $-1 \leq \Re\{s'_k\}, \Im\{s'_k\} \leq 1$ is obtained by normalizing s_k according to $s'_k = s_k / \max\{\max\{|\Re\{\mathbf{s}\}|\}, \max\{|\Im\{\mathbf{s}\}|\}\}$, where \mathbf{s} is the pulse-shaped signal sequence and $|\Re\{\mathbf{s}\}|$ and $|\Im\{\mathbf{s}\}|$ return the absolute value of the real and imaginary part of each element in \mathbf{s} , respectively.

At the receiver, NN4 $f_{\theta_4}: \mathbb{C} \rightarrow \mathcal{M}$ maps the downsampled signal y_k to an M -dimensional probability vector according to $\mathbf{q}_k = f_{\theta_4}(y_k)$, where θ_4 is the set of trainable parameters. The transmitted message is estimated according to $\hat{m}_k = \arg \max_m [\mathbf{q}_k]_m$, where $[\mathbf{x}]_m$ returns the m -th element of \mathbf{x} .

3.2. Optimization procedure

The system is trained in an end-to-end manner by minimizing the cross-entropy loss defined by $\mathcal{J}_{\text{CE}}(\theta_1, \theta_2, \theta_3, \theta_4) = \mathbb{E}\{\log[f_{\theta_4}(y_k)]_{m_k}\}$, where the dependence of $\mathcal{J}_{\text{CE}}(\theta_1, \theta_2, \theta_3, \theta_4)$ on $\theta_1, \theta_2, \theta_3$ is implicit through the distribution of the downsampled signal y_k , which is a function of the channel input $g(\tilde{s}_k)$, where $g(\cdot)$ denotes the transfer function of the DAC, PA and IQM, and \tilde{s}_k is dependent on NNs 1–3 as can be seen in the bottom branch of Fig. 1. In practice, \mathcal{J}_{CE} can be approximated via Monte Carlo simulation according to $\hat{\mathcal{J}}_{\text{CE}}(\theta_1, \theta_2, \theta_3, \theta_4) \approx \frac{1}{B_s} \sum_{k=1}^{B_s} \log[f_{\theta_4}(y_k)]_{m_k}$, where B_s is the mini-batch size. For the optimization, in order to have a faster and more stable convergence, the NNs are first initialized to mimic their model-based counterparts via pre-training. Then, the sets of parameters $\theta_1, \theta_2, \theta_3, \theta_4$ are jointly optimized using the Adam optimizer.

4. Results

We set $M = 64$ and consider a 3-channel system where the guard band between the adjacent channels is ηf_b , where $\eta \geq 0$ and f_b is the symbol rate. The hardware impairment considered in this paper is restricted to the IQM nonlinearity, while it should be noted that the proposed approach can be straightforwardly applied to a more general setup where the other transmitter components are not idealized. As in [3,4], we consider the IQM transfer function $E_{\text{out}} = \sin(E_{\text{in}} \pi/2)$, where E_{in} is the driving signal with a peak voltage V_p . At the receiver, the ADC is implemented as a brick-wall filter (i.e., with $2f_b$ bandwidth) followed by a sampler with rate $2f_b$, and the MF is fixed to a root-raised cosine (RRC) filter, which is also used for PS in the baseline. Furthermore, for the baseline, we use a geometrically-shaped constellation set obtained by training a standard AE [18] over the AWGN channel at SNR = 18 dB, and apply the arcsin with clipping based DPD [3], according to $\tilde{s}_k = \min\{V_{\text{clip}}, \arcsin(s_k)\}$, where V_{clip} is referred to as the clipping factor and $\arcsin(\cdot)$ operates separately on in-phase and quadrature branches, to compensate the IQM nonlinearity. The system performance is evaluated by measuring the achieved SER.

Impact of guard band η : We start by investigating a single-channel scenario. Fig. 2 (a) presents the SER of the proposed system when the receiver MF uses 10% roll-off. For a range of considered V_p , the proposed approach achieves significantly better performance than the considered baseline. However, by looking at the frequency response of the learned PS filter, as shown with the blue dashed curve in Fig. 2 (b), we observe that compared to the RRC filter with 10% roll-off, the learned filter has a significant amount of out-of-band (OOB) energy, which will introduce significant ICI with narrowly-spaced neighbouring channels and make it unsuitable for superchannel systems. In contrast, when training the proposed AE in a 3-channel system with $\eta = 0.05$, Fig. 2 (b) shows that the learned filter restricts the OOB energy and has a narrower frequency response than the RRC filter, indicating that the trainable filter learns to limit ICI.

SER analysis: We now evaluate the performance of the proposed system setting the receiver MF roll-off factor to 10% and 1%. The achieved SER for the central channel is shown in Fig. 3. As a reference, the SER performance of the baseline scheme is also shown. We remark that the clipping factor V_{clip} and V_p are optimized for the baseline scheme, while V_p is set to 1 in the proposed scheme for simplicity. Potentially, the performance of the

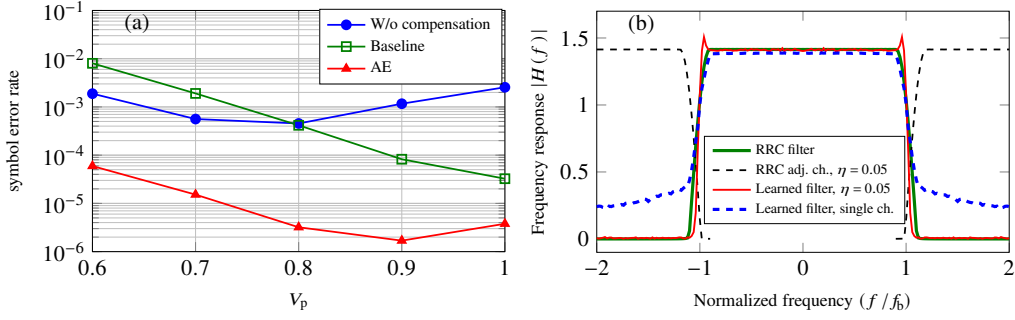


Fig. 2. (a): SER performance versus V_p for the single channel scenario, the blue curve corresponds to the baseline setup but without applying DPD; (b): Frequency response of the learned filters when the receiver MF roll-off factor is set to 10%. The frequency response of the RRC filter with 10% roll-off is also shown as a reference.

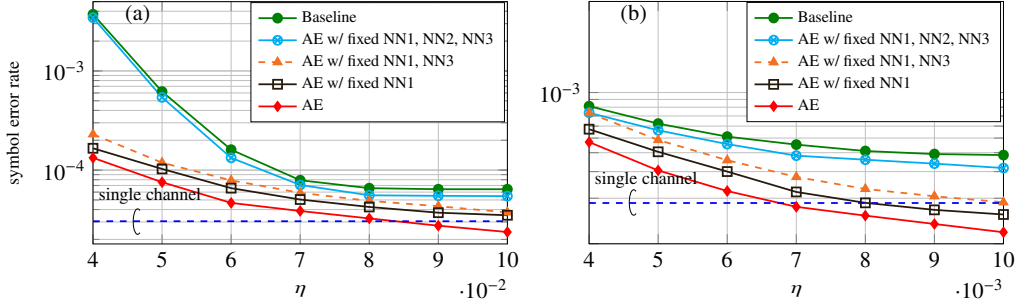


Fig. 3. SER of the central channel of the proposed scheme and the baseline when the receiver MF roll-off factor set to (a) 10% roll-off and (b) 1% roll-off. The blue dashed curve corresponds to the SER of the baseline for a single channel scenario.

proposed scheme can be further improved by optimizing V_p —the optimal performance for the single channel case is achieved at $V_p = 0.9$ (see Fig. 2 (a)). For roll-off factors of 10% (Fig. 3(a)) and 1% (Fig. 3(b)), the proposed approach outperforms the baseline scheme over all considered guard bands. More importantly, compared to the baseline scheme, the guard band for the proposed scheme can be significantly reduced with limited impact on the SER performance—for the target SER where the baseline performance starts to saturate, the guard band can be reduced by around 37% for 10% roll-off and around 50% for 1% roll-off.

Ablation study: In order to quantify the origin of the performance gains, we carry out an ablation study by first freezing all the pre-trained NNs and individually unfreezing the NNs in the order of NN4, NN2, NN3, and NN1. Fig. 3 shows that the SER performance of proposed system improves every time one more NN is made trainable, indicating that the performance improvement of the proposed system can be attributed to the joint optimization of the mapper, the PS filter, the nonlinearity compensator (i.e., the DPD), and the de-mapper.

5. Conclusion

We have proposed an approach for high SE superchannel systems using an AE, where the transmitter network design follows the architecture of conventional systems. The resulting system achieves significantly better performance than the considered baseline scheme, and allows to increase the SE of superchannel systems by reducing the channel spacing without SER performance degradation.

Acknowledgements: This work was supported by the Knut and Alice Wallenberg Foundation, grant No. 2018.0090, and the Swedish Research Council under grant No. 2018-0370.

References

1. G. Bosco *et al.*, "Investigation on the robustness of a nyquist-WDM terabit superchannel to transmitter and receiver non-idealities," in *Proc. ECOC*, 2010.
2. C. Liu *et al.*, "Joint digital signal processing for superchannel coherent optical communication systems," *Optics Express*, vol. 21, no. 7, pp. 8342–8356, 2013.
3. V. Curri *et al.*, "Optimization of DSP-based nyquist-WDM PM-16QAM transmitter," in *Proc. ECOC*, 2012.
4. Y. Tang *et al.*, "Coherent optical OFDM transmitter design employing predistortion," *IEEE Photon. Technol. Lett.*, vol. 20, no. 11, pp. 954–956, 2008.
5. G. Khanna *et al.*, "A robust adaptive pre-distortion method for optical communication transmitters," *Photon. Technol. Lett.*, vol. 28, no. 7, pp. 752–755, 2015.
6. P. W. Berenguer *et al.*, "Nonlinear digital pre-distortion of transmitter components," *J. light. technol.*, vol. 34, no. 8, pp. 1739–1745, 2015.
7. R. Elschner *et al.*, "Improving achievable information rates of 64-GBd PDM-64QAM by nonlinear transmitter predistortion," in *Proc. OFC*, 2018.
8. Y. Yoffe *et al.*, "Low-resolution digital pre-compensation enabled by digital resolution enhancer," *J. Light. Technol.*, vol. 37, no. 6, pp. 1543–1551, 2019.
9. N. Benvenuto *et al.*, "A neural network approach to data predistortion with memory in digital radio systems," in *Proc. ICC*. IEEE, 1993, pp. 232–236.
10. C. Tarver *et al.*, "Design and implementation of a neural network based predistorter for enhanced mobile broadband," in *Proc. SiPS*, 2019, pp. 296–301.
11. T. Gotthans *et al.*, "Digital predistortion with advance/delay neural network and comparison with volterra derived models," in *Proc. PIMRC*, 2014, pp. 811–815.
12. C. Tarver *et al.*, "Neural network DPD via backpropagation through a neural network model of the pa," in *Proc. ACSSC*. IEEE, 2019, pp. 358–362.
13. G. Paryanti *et al.*, "Recurrent neural network for pre-distortion of combined nonlinear optical transmitter impairments with memory," in *Proc. SPPCom*, 2018.
14. M. Schaedler *et al.*, "AI-based digital predistortion for IQ mach-zehnder modulators," in *Proc. ACP*, 2019.
15. M. Abu-Romoh *et al.*, "Neural-network-based pre-distortion method to compensate for low resolution DAC nonlinearity," in *Proc. ECOC*, 2019.
16. G. Paryanti *et al.*, "A direct learning approach for neural network based pre-distortion for coherent nonlinear optical transmitter," *J. Light. Technol.*, 2020.
17. V. Bajaj *et al.*, "Single-channel 1.61 Tb/s optical coherent transmission enabled by neural network-based digital pre-distortion," in *Proc. ECOC*, 2020.
18. T. O'Shea *et al.*, "An introduction to deep learning for the physical layer," *Trans. on Cogn. Commun. and Netw.*, vol. 3, no. 4, pp. 563–575, 2017.
19. T. Uhlemann *et al.*, "Deep-learning autoencoder for coherent and nonlinear optical communication," in *21th ITG-Symposium on Photonic Networks*, 2020.